First-in-Human Study of ^{18}F-SynVesT-2: An SV2A PET Imaging Probe with Fast Brain Kinetics and High Specific Binding

Lindsey R. Drake, Yanjun Wu, Mika Naganawa, Ruth Asch, Chao Zheng, Soheila Najafzadeh, Richard Pracitto, Marcel Lindemann, Songye Li, Jim Ropchan, David Labaree, Paul R. Emery, Mark Dias, Shannan Henry, Nabeel Nabulsi, David Matuskey, Ansel T. Hillmer, Jean-Dominique Gallezot, Richard E. Carson, Zhengxin Cai, and Yiyun Huang

Yale PET Center, New Haven, Connecticut

PET imaging of synaptic vesicle glycoprotein 2A allows for noninvasive quantification of synapses. This first-in-human study aimed to evaluate the kinetics, test–retest reproducibility, and extent of specific binding of a recently developed synaptic vesicle glycoprotein 2A PET ligand, (*R*)-4-(3-(^{18}F-fluoro)phenyl)-1-((3-methylpyridin-4-yl)methyl)-pyrrolidine-2-one (^{18}F-SynVesT-2), with fast brain kinetics. **Methods:** Nine healthy volunteers participated in this study and were scanned on a High Resolution Research Tomograph scanner with ^{18}F-SynVesT-2. Five volunteers were scanned twice on 2 different days. Five volunteers were rescanned with preinjected levetiracetam (20 mg/kg, intravenously). Arterial blood was collected to calculate the plasma free fraction and generate the arterial input function. Individual MR images were coregistered to a brain atlas to define regions of interest for generating time–activity curves, which were fitted with 1- and 2-tissue-compartment (1TC and 2TC) models to derive the regional distribution volume (V_T). The regional nondisplaceable binding potential (BP_{ND}) was calculated from 1TC V_T, using the centrum semiovale (CS) as the reference region. **Results:** ^{18}F-SynVesT-2 was synthesized with high molar activity (187 ± 69 MBq/nmol, n = 19). The parent fraction of ^{18}F-SynVesT-2 in plasma was 28% ± 8% at 30 min after injection, and the plasma free fraction was high (0.29 ± 0.04). ^{18}F-SynVesT-2 entered the brain quickly, with an SUV_{peak} of 8 within 10 min after injection. Regional time–activity curves fitted well with both the 1TC and the 2TC models; however, V_T was estimated more reliably using the 1TC model. The 1TC V_T ranged from 1.9 ± 0.2 mL/cm^3 in CS to 7.6 ± 0.8 mL/cm^3 in the putamen, with low absolute test–retest variability (6.0% ± 3.6%). Regional BP_{ND} ranged from 1.76 ± 0.21 in the hippocampus to 3.06 ± 0.29 in the putamen. A 20-min scan was sufficient to provide reliable V_T and BP_{ND}. **Conclusion:** ^{18}F-SynVesT-2 has fast kinetics, high specific uptake, and low nonspecific uptake in the brain. Consistent with the nonhuman primate results, the kinetics of ^{18}F-SynVesT-2 is faster than the kinetics of ^{11}C-UCB-J and ^{18}F-SynVesT-1 in the human brain and enables a shorter dynamic scan to derive physiologic information on cerebral blood flow and synapse density.

Key Words: SV2A; brain PET; ^{18}F-SynVesT-2; first-in-human; kinetic modeling; dosimetry

J Nucl Med 2024; 65:462–469
DOI: 10.2967/jnumed.123.266470

The ability of synapses to adapt and change is essential for learning and memory, and the capacity for synaptic plasticity can be influenced by environmental factors (*1*). Synaptic vesicle glycoprotein 2A (SV2A) is ubiquitously expressed in presynaptic vesicles throughout the central nervous system and thus considered to be a useful indirect measure of synaptic density. PET with radiotracers targeting SV2A therefore provides a minimally invasive method that is suitable for the longitudinal and quantitative assessment of synaptic density, making possible investigations of synapse dynamics during disease pathogenesis and in response to treatment with experimental drugs (*2–9*). In a SV2A PET imaging study in Alzheimer disease patients and healthy controls, the team of Chen et al. demonstrated that a single dynamic SV2A PET scan provides information on both cerebral blood flow, which is related to neuronal activity, and synaptic density (*10–12*). The commonly used SV2A PET ligands (*R*)-1-((3-[^{11}C]methylpyridin-4-yl)methyl)-4-(3,4,5-trifluorophenyl)pyrrolidin-2-one (^{11}C-UCB-J) and (*R*)-4-(3-fluoro-5-(fluoro-^{18}F)phenyl)-1-((3-methylpyridin-4-yl)methyl)pyrrolidin-2-one (^{18}F-SynVesT-1) (formerly referred to as ^{18}F-SDM-8) need 60-min dynamic scans to reliably generate parameters related to cerebral blood flow and synaptic density (*3–5*). It is desirable to maximize the information gained through 1 dynamic PET scan with a shorter scan duration, as shorter scans would improve subject compliance and imaging throughput, reduce motion effects, and enable the study of broader patient populations. One common strategy to improve kinetics without compromising specific binding signal in the brain is to lower the binding affinity and increase the nondisplaceable brain free fraction (f_{ND}) by fine-tuning the physicochemical properties of the imaging ligands. The ^{18}F-labeled monofluorinated UCB-J analog, (*R*)-4-(3-(^{18}F-fluoro)phenyl)-1-((3-methylpyridin-4-yl)methyl)-pyrrolidine-2-one (^{18}F-SynVesT-2, formerly referred to as ^{18}F-SDM-2), with slightly reduced binding affinity and hydrophobicity, exhibited faster brain kinetics, lower nonspecific binding, and high specific binding in nonhuman primate brains (*13*). Therefore, we hypothesized that ^{18}F-SynVesT-2 would allow for shorter dynamic scanning for reliable estimation of both synapse density and cerebral blood flow index, with high specific binding in the human brain. We tested this hypothesis in this first-in-human study of ^{18}F-SynVesT-2 on healthy volunteers at baseline and under blocking conditions using levetiracetam.

MATERIALS AND METHODS

Radiotracer Synthesis

^{18}F-SynVesT-2 was synthesized following a previously published protocol with minor modifications (*13*). The supplemental

Received Jul. 31, 2023; revision accepted Dec. 19, 2023.
For correspondence or reprints, contact Yiyun (Henry) Huang (henry.huang@yale.edu) or Zhengxin Cai (jason.cai@yale.edu).
Published online Feb. 15, 2024.

materials provide more details (available at http://jnm.snmjournals.org) (*14–23*).

Radiation Dosimetry Study on Nonhuman Primates

The study was performed under a protocol approved by the Yale University Institutional Animal Care and Use Committee.

Healthy Volunteers

Nine healthy volunteers participated (6 men and 3 women; age, 43 ± 12 y [range, 27–56 y]; weight, 77 ± 14 kg [range, 52–111 kg]). Two of the subjects underwent 3 PET scans, that is, 2 baseline scans and 1 blocking scan. All participants underwent a medical assessment including screening laboratory values and were free of present or past major medical illnesses, including significant neurologic and psychiatric disorders. Additionally, they reported no history of substance use and had no contraindications to MRI scans. The subject demographics and tracer injection parameters are shown in Supplemental Table 1. This PET imaging study was performed under a protocol approved by the Yale University Human Investigation Committee (approval 2000025929), the Yale Radiation Safety Committee, and the Yale MRI Safety Committee and was in accordance with U.S. federal policy for the protection of human research subjects contained in Title 45, part 46, of the *Code of Federal Regulations*. We obtained written informed consent from all participants after they had received a complete explanation of the study procedure.

Human Brain Imaging Studies

MRI. Each subject underwent T1-weighted MRI for coregistration with the PET images.

Human Brain PET Imaging. Human brain PET scans were performed on a High Resolution Research Tomograph (Siemens Medical Systems) and followed a previously published scanning protocol (*3,5*).

Blood Analysis. Blood analysis experiments followed a previously published scanning protocol (*3–5*).

Image Registration and Definitions of Regions of Interest (ROIs). Image registration and definitions of ROIs followed previously published scanning protocols (*3–5*). The ROI for the centrum semiovale (CS) was based on a 2-cm^3 CS region defined in Montreal Neurologic Institute space, as previously described (*2*).

Quantitative Analysis

Two outcome measures—distribution volume (V_T) and K_1—were calculated with the 1-tissue-compartment (1TC) model and the 2-tissue-compartment (2TC) model, without the cerebral blood fraction parameter. The relative performance of the 1TC and 2TC models was based on the Akaike information criterion (AIC), *F* tests, and comparison of V_T and K_1 and their reproducibility. Percentage SE (%SE) was estimated from the theoretic parameter covariance matrix. Comparison of K_1 and V_T calculated by different models was limited to those that were reliably estimated—for example, with %SE less than 10%. The time stability of 1TC V_T and K_1 was evaluated, with or without counting for the fitted blood volume in the brain. Guo plot analysis was used to compare the in vivo K_d of the SV2A PET tracers (*23*).

The CS was used as the reference region to compute regional nondisplaceable binding potential (BP_{ND}) from V_T. The Lassen plot was applied to compute levetiracetam occupancy and nondisplaceable distribution volume (V_{ND}). V_{ND} was compared with the V_T of the CS at baseline to test the suitability of the CS as a reference region, as previously done with ^{18}F-SynVesT-1 (*4,5*). The minimum scan duration for V_T was evaluated by fitting the regional time–activity curves for PET data with truncated acquisition times ranging from 20 to 90 min. The ratio of the regional V_T from the truncated scan to that from the 90-min measurement was computed for each ROI. The minimum scan duration for BP_{ND} was evaluated with truncated scan times ranging from 20 to 90 min in 10-min increments. The minimum acceptable acquisition time was assessed for each region according to the following criteria: an average ratio of 95%–105%, and an interindividual SD of less than 10% for the ratio.

An additional, simplified, outcome measure—the SUV ratio (SUVR)—was evaluated. Static SUVR–1, equivalent to BP_{ND} at equilibrium, was computed for 7 time windows of 30-min duration (0–30, 10–40, 20–50, 30–60, 40–70, 50–80, and 60–90) and compared with BP_{ND} calculated from the regional V_T ratio (target/reference) − 1.

Test–Retest Evaluation

The reproducibility of the obtained outcome parameters was examined by calculation of the relative test–retest variability (TRV) and absolute TRV (aTRV). TRV was calculated as 2 × (retest − test)/(test + retest), and aTRV was calculated as 2 × |retest − test|/(test + retest).

RESULTS

PET Tracer Synthesis and Quality Control

The synthesis process of ^{18}F-SynVesT-2 was validated in 3 consecutive validation runs, and the final products met the preset quality control criteria (Supplemental Table 2 shows the quality control results of 3 validation runs). The production of ^{18}F-SynVesT-2 for human use followed the same protocol as used in the validation runs, and the final product quality was consistent. The radiochemical purity of ^{18}F-SynVesT-2 was over 99%. The molar activity at the end of synthesis was 187 ± 69 MBq/nmol (n = 19).

Dosimetry Calculation

The injected activity in the nonhuman primate dosimetry scans was 138.8 ± 57.7 MBq (n = 4). The maximum permissible single-study dose of ^{18}F-SynVesT-2 was calculated from the averaged organ radiation exposure levels to remain below the limit in title 21, part 361.1, of the *Code of Federal Regulations* (for a single study, 50 mSv per organ or 30 mSv to selected organs undergoing rapid cell division, whichever is less). The urinary bladder wall was determined to be the dose-limiting organ for both men and women, with a maximum permissible single-study dose of 257.9 MBq for a woman and 322.6 MBq for a man using the no-bladder-void model. Using the voiding model with a 3.5-h voiding interval, the maximum single-study doses for men and women were 719.6 and 414.4 MBq, respectively, with the urinary bladder wall as the dose-limiting organ (Supplemental Tables 3 and 4).

Human Injection Parameters

The injected radioactivity of ^{18}F-SynVesT-2 was 178.9 ± 4.2 MBq (range, 172.8–183.9 MBq; n = 5) for the test PET scans, 181.7 ± 5.1 MBq (range, 175.4–186.1 MBq; n = 5) for the retest PET scans, and 184.0 ± 3.9 MBq (range, 179.1–188.0 MBq; n = 5) for the blocking PET scans (Supplemental Table 1). The injected mass dose of SynVesT-2 was 0.40 ± 0.19 μg (range, 0.20–0.99 μg; n = 19), corresponding to 5.4 ± 3.6 ng/kg (n = 19). There was no statistically significant difference in the injected radioactivity dose, molar activity, or injected mass between the test and retest conditions.

Safety

No significant clinical changes were observed with the administration of ^{18}F-SynVesT-2 in this study. There were no adverse events or clinically detectable pharmacologic effects reported in any of the subjects. No significant changes in vital signs were observed. The subjects completed their scans without reporting discomfort that would warrant secession from scanning.

Blood Analysis

The mean extraction efficiency and high-performance liquid chromatography fraction recovery value were more than 97% at all time points. Representative high-performance liquid radiochromatograms from plasma samples obtained at 8, 15, 60, and 120 min after injection of ^{18}F-SynVesT-2 in 1 volunteer are displayed in Figure 1A. After injection of ^{18}F-SynVesT-2, only 1 major radiometabolite fraction was detected during the course of the PET measurement. The radiometabolite fraction had a retention time of about 7.5 min, eluting earlier than ^{18}F-SynVesT-2 (~11 min). This is similar to ^{18}F-SynVesT-1, which also features 1 major plasma radiometabolite peak (*5*). Figure 1B displays the parent fractions of ^{18}F-SynVesT-2 over the time course of the baseline and blocking PET measurements. There was a trend toward slightly higher parent fractions during the blocking scans than during the baseline scans, albeit the differences were not statistically significant after correction for multiple comparisons. However, there was a significant difference in the mean area under the curve of the ^{18}F-SynVesT-2 plasma concentration from 0 to 90 min after injection at baseline (area under the curve, 52.4 ± 1.3 SUV × min; n = 14) and under blocking conditions (area under the curve, 69.0 ± 1.8 SUV × min; n = 5; 2-tailed $P < 0.005$, paired t test) (Figs. 1C and 1D). The observed higher area under the curve of plasma concentration under blocking conditions is not uncommon among brain PET tracers. The plasma free fraction (f_p) of ^{18}F-SynVesT-2 was high and could be reliably measured at 0.29 ± 0.04 (range, 0.24–0.39; n = 19). The f_p of ^{18}F-SynVesT-2 was not changed during the baseline and blocking scans (P = 0.33, paired t test; n = 3 pairs).

Brain Distribution and Kinetics

The regional brain distribution of ^{18}F-SynVesT-2 was similar to that of ^{18}F-SynVesT-1 and ^{11}C-UCB-J, with high uptake in gray matter and low uptake in white matter. Typical time–activity curves from a representative subject as the 1TC model fitted curves are shown in Figure 2. SUV in brain regions peaked at 5–10 min after injection and ranged from 5 to 9 in gray matter. Uptake in white matter (CS) was considerably lower than that in gray matter. A steady decline in regional radioactivity was observed from 10 to 20 min after injection. The summed SUV images from 40 to 60 min after injection showed high-resolution mapping of SV2A in the human brain (Fig. 3).

The 1TC model described the regional time–activity curves well, and kinetic parameters (both K_1 and V_T) were reliably estimated (%SE < 10% for 418/418 ROIs). On the basis of the AIC and F test results, the 2TC model fits the time–activity curves better than 1TC model does (for the F test, $P < 0.05$ in 126/209 ROIs; the 2TC AIC value was lower than the 1TC AIC value, $P < 0.001$). However, using 2TC modeling, the K_1 could not be reliably estimated for 19% of the analyzed ROIs (%SE > 100% for 39/209 ROIs), and the V_T could not be reliably estimated for 28% of the analyzed ROIs (%SE > 100% for 58/209 ROIs). This finding is consistent with previous ^{11}C-UCB-J data (*3*). Similarly, the 1TC model with blood volume correction fits the time–activity curves better than the 1TC model does without blood volume correction (for the F test, $P < 0.05$ in 80/209 ROIs; the 1TC with blood volume correction AIC value was lower than the 1TC without blood volume correction AIC value, $P < 0.001$). However, adding blood volume correction slightly degraded the reliability of the V_T estimates (%SE > 100% for 21/209 ROIs), and V_T estimates were similar with and without blood volume correction (V_T estimates were only −2% ± 3% lower with blood volume correction, n = 209). Therefore, the 1TC model without blood volume correction was used as the preferred model for the analysis of 90-min datasets. The mean K_1 (mL/cm^3/min) estimated from 1TC ranged from 0.11 ± 0.02 in the CS to 0.38 ± 0.06 in the putamen (Table 1). These K_1 (mL/cm^3/min) values are similar to those

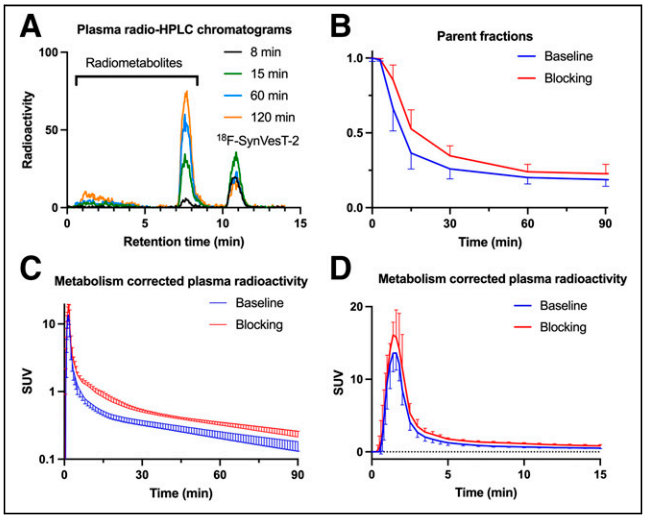

FIGURE 1. Representative radio–high-performance liquid chromatograms of plasma content at 8, 15, 60, and 120 min after intravenous injection of ^{18}F-SynVesT-2 in humans, showing radiometabolite peaks with higher hydrophilicity (A), parent fraction of ^{18}F-SynVesT-2 in plasma over time under baseline (n = 14) and blocking (n = 5) conditions (B), and concentration of ^{18}F-SynVesT-2 (mean ± SD) in plasma over time under baseline (n = 14) and blocking conditions (n = 5) from 0 to 90 min after injection (C) and from 0 to 15 min after injection (D). HPLC = high-performance liquid chromatography.

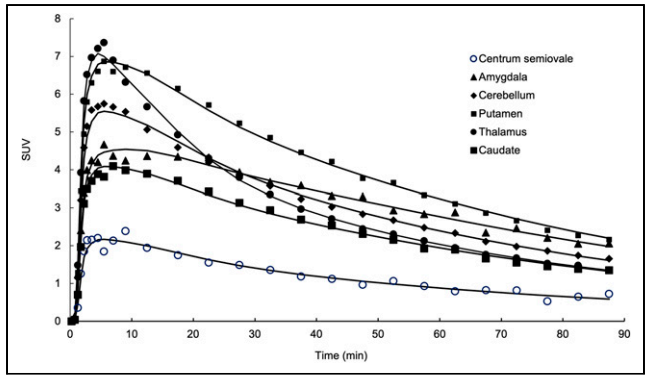

FIGURE 2. Time–activity curves derived from single representative ^{18}F-SynVesT-2 baseline scan. Time–activity curves for amygdala, cerebellum, putamen, thalamus, caudate nucleus, and CS are displayed with 1TC model fitted curves (black solid lines).

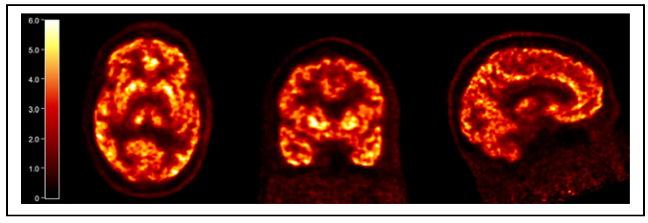

FIGURE 3. Summed SUV PET images of representative ^{18}F-SynVesT-2 baseline scan, from 40 to 60 min after injection.

TABLE 1
Kinetic Parameters of ^{18}F-SynVesT-2 Under Baseline and Blocking Conditions Derived with 1TC Model from 90-Minute Time–Activity Curves

	K_1 (mL/cm^3/min)		K_2 (min^{-1})		V_T (mL/cm^3)	
Region	Baseline	Blocking	Baseline	Blocking	Baseline	Blocking
Amygdala	0.25 ± 0.05	0.24 ± 0.05	0.037 ± 0.006	0.12 ± 0.02	6.72 ± 0.74	2.06 ± 0.26
CS	0.11 ± 0.02	0.09 ± 0.01	0.059 ± 0.009	0.07 ± 0.01	1.88 ± 0.23	1.44 ± 0.14
Caudate nucleus	0.28 ± 0.06	0.26 ± 0.06	0.050 ± 0.007	0.15 ± 0.03	5.64 ± 0.75	1.80 ± 0.22
Cerebellum	0.29 ± 0.04	0.26 ± 0.03	0.052 ± 0.005	0.14 ± 0.02	5.69 ± 0.65	1.80 ± 0.21
Frontal lobe	0.36 ± 0.05	0.3 ± 0.05	0.053 ± 0.006	0.15 ± 0.03	6.74 ± 0.85	2.02 ± 0.27
Hippocampus	0.24 ± 0.03	0.23 ± 0.03	0.046 ± 0.006	0.13 ± 0.02	5.17 ± 0.54	1.81 ± 0.20
Occipital lobe	0.35 ± 0.06	0.33 ± 0.05	0.050 ± 0.008	0.16 ± 0.03	6.96 ± 0.79	2.10 ± 0.28
Parietal lobe	0.35 ± 0.06	0.31 ± 0.05	0.050 ± 0.007	0.15 ± 0.03	6.91 ± 0.85	2.05 ± 0.30
Putamen	0.38 ± 0.06	0.35 ± 0.06	0.051 ± 0.008	0.16 ± 0.03	7.60 ± 0.78	2.27 ± 0.29
Temporal lobe	0.33 ± 0.05	0.30 ± 0.05	0.045 ± 0.007	0.14 ± 0.03	7.43 ± 0.87	2.18 ± 0.30
Thalamus	0.36 ± 0.05	0.32 ± 0.04	0.065 ± 0.007	0.17 ± 0.03	5.57 ± 0.63	1.91 ± 0.20

n = 9 subjects.

of ^{18}F-SynVesT-1 (range, 0.11–0.37) and ^{11}C-UCB-J (range, 0.13–0.39) (*3,5*). The mean k_2 (min^{-1}) ranged from 0.037 ± 0.006 in the amygdala to 0.065 ± 0.007 in the thalamus (Table 1). ^{18}F-SynVesT-2 features faster kinetics as evidenced by the higher washout rate than for ^{18}F-SynVesT-1 (mean k_2 [min^{-1}], 0.014 in the amygdala to 0.032 in the CS) (*5*). The mean k_2 ratios of ^{18}F-SynVesT-2 to those of ^{18}F-SynVest-1 and ^{11}C-UCB-J were 2.5 ± 0.2 and 2.8 ± 0.2, respectively, indicating that the brain kinetics of ^{18}F-SynVesT-2 is 2.5-fold and 2.8-fold faster than the brain kinetics of ^{18}F-SynVesT-1 and ^{11}C-UCB-J, respectively. Correspondingly, the mean V_T (mL/cm^3) ranged from 1.9 in the CS to 7.6 in the putamen (Table 1), which are lower than those of ^{18}F-SynVesT-1 (3.5 in the CS to 19 in the putamen) (*5*) and ^{11}C-UCB-J (5.3–22) (*3*), as expected from the faster washout rate constant, k_2.

Blocking studies with levetiracetam (20 mg/kg intravenously, 3 h before tracer injection) were performed on 5 individuals to demonstrate the in vivo specific binding of ^{18}F-SynVesT-2 to SV2A. Reduction in ^{18}F-SynVesT-2 uptake was noticeable across brain regions, with the least change in the CS. The mean V_T values (mL/cm^3) for the blocking scans were 1.44 ± 0.14 in the CS to 2.27 ± 0.29 in the putamen (Table 1). On the basis of the Lassen plots, SV2A occupancy by levetiracetam was 85% ± 3% (Fig. 4 Supplemental Tables 5 and 6). This level of occupancy is similar to that measured with ^{18}F-SynVesT-1 (85.3%) or ^{11}C-UCB-J (82.5%) under identical blocking conditions (*5*). The V_{ND} determined as the x-intercepts from the Lassen plots was 1.30 ± 0.10 mL/cm^3 (n = 5), which is significantly lower than those of ^{11}C-UCB-J and ^{18}F-SynVesT-1 (3.13 ± 0.41 mL/cm^3, n = 4, and 2.38 ± 0.33 mL/cm^3, n = 4, respectively; $P < 0.0001$, 1-way ANOVA), presumably because of the higher hydrophilicity of ^{18}F-SynVesT-2 (*5*). The V_{ND} of gray matter was lower than the baseline CS V_T by 26% ± 4% for ^{18}F-SynVesT-2 (n = 5), which is lower than those for ^{18}F-SynVesT-1 (32% ± 16%, n = 4) and ^{11}C-UCB-J (29% ± 13%, n = 4) but not significantly different among the 3 tracers (P = 0.74, 1-way ANOVA), likely because of the small sample sizes.

When the baseline CS V_T was used as the reference value, the BP_{ND} ranged from 1.76 ± 0.21 in the hippocampus to 3.06 ± 0.29 in the putamen for ^{18}F-SynVesT-2 (Table 2). This range is lower than those of ^{18}F-SynVesT-1 (2.7 ± 0.4 in the hippocampus to 4.5 ± 0.5 in the putamen: Supplemental Fig. 1) and ^{11}C-UCB-J (2.1 in the hippocampus to 3.7 in the putamen).

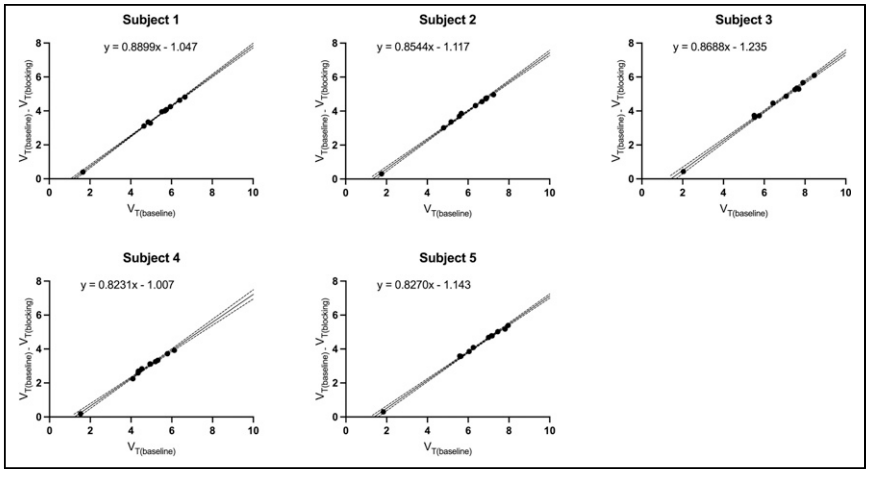

FIGURE 4. Lassen plots of ^{18}F-SynVesT-2 in 5 subjects with baseline and levetiracetam (20 mg/kg, intravenously) blocking PET scans. Data are in mL/cm^3.

TABLE 2
BP_{ND} of ^{18}F-SynVesT-2 Under Baseline and Blocking Conditions, and TRV of BP_{ND}

	BP_{ND}		Test–retest	
Region	Baseline (n = 9 subjects, 14 scans)	Blocking (n = 5)	TRV (n = 5)	aTRV (n = 5)
Amygdala	2.59 ± 0.31	0.43 ± 0.08	0.26% ± 9.90%	7.38% ± 5.09%
Caudate nucleus	2.03 ± 0.41	0.25 ± 0.1	−2.73% ± 14.87%	13.34% ± 5.12%
Cerebellum	2.03 ± 0.18	0.25 ± 0.04	−2.62% ± 10.93%	9.77% ± 4.93%
Frontal lobe	2.59 ± 0.34	0.4 ± 0.06	−0.71% ± 11.78%	9.96% ± 5.29%
Hippocampus	1.76 ± 0.21	0.26 ± 0.07	3.08% ± 15.18%	12.40% ± 5.09%
Occipital lobe	2.72 ± 0.36	0.46 ± 0.09	0.74% ± 13.34%	10.42% ± 5.27%
Parietal lobe	2.69 ± 0.37	0.42 ± 0.09	−0.33% ± 15.38%	13.12% ± 6.88%
Putamen	3.06 ± 0.29	0.58 ± 0.1	−1.28% ± 10.59%	9.36% ± 4.17%
Temporal lobe	2.97 ± 0.37	0.51 ± 0.1	0.46% ± 12.72%	10.69% ± 5.44%
Thalamus	1.97 ± 0.24	0.33 ± 0.07	−0.47% ± 17.23%	14.15% ± 8.50%

Data are mean ± SD.

This finding is consistent with the prediction from the Guo plots. A global decrease (~85%) in BP_{ND} was observed in the blocking studies, consistent with the Lassen plot analysis results. Blocking BP_{ND} ranged from 0.25 ± 0.10 in the caudate nucleus to 0.58 ± 0.1 in the putamen.

The time stability of K_1 and V_T was investigated in shorter scan increments ranging from 20 to 90 min. Both K_1 and V_T estimates were stable down to 20 min of scan time and were within 10% of the 90-min data (Fig. 5). The minimum dynamic scan time for stable V_T estimates was 60 min for ^{11}C-UCB-J and ^{18}F-SynVesT-1, consistent with the faster kinetics and higher k_2 for ^{18}F-SynVesT-2 in the human brain. The time stability of V_T estimates would be slightly further improved by including blood volume correction in the model, whereas the time stability of K_1 estimates would be degraded slightly (Supplemental Fig. 2). The time stability of BP_{ND} was also investigated, and BP_{ND} derived from the minimum scan time of 20 min deviated by only –0.9% ± 9.0% from values estimated using the full 90-min dynamic imaging dataset (Fig. 6). This is an obvious improvement over ^{11}C-UCB-J and ^{18}F-SynVesT-1, both of which require longer dynamic scan times (Supplemental Figs. 3 and 4).

To evaluate the measurement robustness of the baseline scans using ^{18}F-SynVesT-2, we calculated the TRV and aTRV of the key 1TC modeling parameters from the test–retest scans of 5 subjects. Table 3 lists the test–retest reproducibility results for each region for 1TC K_1 and V_T. The global mean aTRV of V_T for ^{18}F-SynVesT-2 was 6.0% (range, 4.7%–7.2%), which was similar to the values for ^{18}F-SynVesT-1 (global mean, 5.8%; range, 4%–8%) and ^{11}C-UCB-J (global mean, 4.4%; range, 3%–9%) (*3,4*). The mean regional aTRV for ^{18}F-SynVesT-2 BP_{ND} was 10.8% ± 1.9%, ranging from 7.8% to 13.7% (Table 2), which is also comparable to the values for ^{11}C-UCB-J and ^{18}F-SynVesT-1 (*4*). Note that the test–retest scans for ^{18}F-SynVesT-2 and ^{18}F-SynVesT-1 were performed on different days, whereas the test–retest scans for ^{11}C-UCB-J were on the same day.

To determine the suitable imaging window for static scans using SUVR–1 as a surrogate of BP_{ND} from dynamic scans, we compared the averaged SUVR–1 using CS as the reference region at different 30-min time windows with the BP_{ND} calculated using 90 min of dynamic scan data (Fig. 7). An optimal imaging window from 20 to 50 min after injection was found to provide SUVR–1 s nearly identical to BP_{ND}, with a mean difference of −0.3% ± 2.6% from the BP_{ND}. This optimal static imaging window is earlier than that for ^{11}C-UCB-J and ^{18}F-SynVesT-1 (60–90 min after injection), as expected from the faster kinetics of ^{18}F-SynVesT-2. Analysis of individual brain regions indicated that for brain regions other than the thalamus, the averaged SUVR–1 of early time windows underestimated BP_{ND}, whereas the SUVR–1 of late time windows overestimated BP_{ND} (Supplemental Fig. 5).

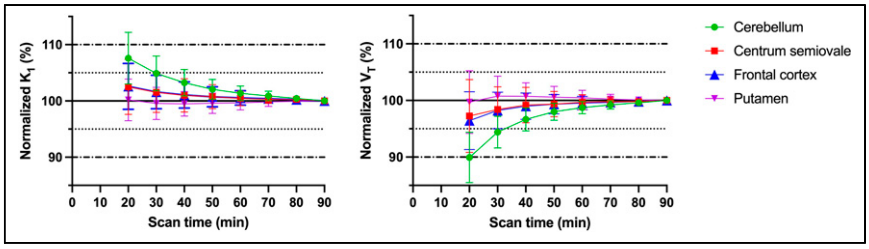

FIGURE 5. Time stability analyses of outcome parameters K_1 and V_T of ^{18}F-SynVesT-2. K_1 and V_T were calculated using 1TC model on data from different scan times and divided by corresponding values measured using 90 min of PET data.

DISCUSSION

After the discovery and development of the PET ligand ^{11}C-UCB-J, which binds specifically to SV2A, researchers in the field of brain PET imaging have studied SV2A changes noninvasively in a variety of neurodegenerative and neuropsychiatric diseases (*11,12,24–32*). However, the currently used SV2A PET ligands, ^{11}C-UCB-J and ^{18}F-SynVesT-1 (^{18}F-SDM-8), need at least 60–90 min of dynamic scan data to reliably derive the index of the cerebral blood

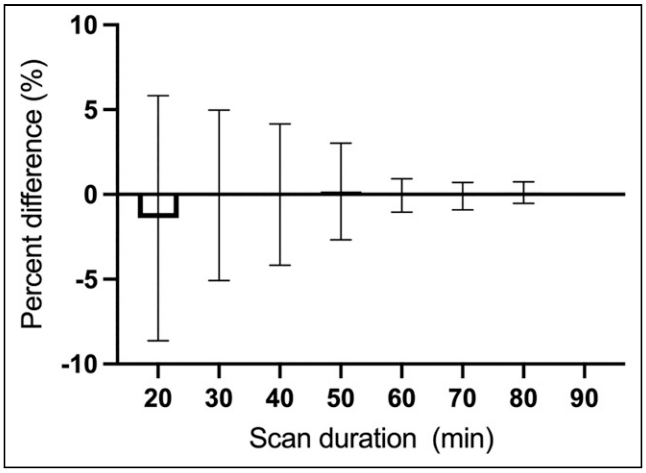

FIGURE 6. Time stability of ^{18}F-SynVesT-2 baseline BP_{ND} using CS as reference region. Shown are percentage differences between BP_{ND} calculated using different scan durations at 10-min increments and BP_{ND} calculated using 90 min of scan data. Data are mean and SD for 9 subjects and 14 scans.

flow and synaptic density. We discovered a new SV2A PET ligand, ^{18}F-SynVesT-2 (^{18}F-SDM-2), which has faster kinetics in nonhuman primate brains (*13*). The aim of this study was to evaluate ^{18}F-SynVesT-2 in healthy human subjects in comparison with ^{11}C-UCB-J and ^{18}F-SynVesT-1 to see whether it is possible to use ^{18}F-SynVesT-2 to shorten the scanning time required for dynamic SV2A PET while getting quantitative information on synapse density and cerebral blood flow index.

Similar to ^{11}C-UCB-J and ^{18}F-SynVesT-1, the brain time–activity curves of ^{18}F-SynVesT-2 are well described by the simple 1TC model, without counting for the cerebral blood fraction. The test–retest repeatability of ^{18}F-SynVesT-2 V_T is excellent, with aTRV below 8% for all brain regions analyzed. Because of the faster clearance from the brain, the 1TC V_T of ^{18}F-SynVesT-2 is consistently lower than that of ^{11}C-UCB-J and ^{18}F-SynVesT-1. Though we did not identify the major radiometabolite of ^{18}F-SynVesT-2 in the plasma, it is likely to be its *N*-oxide pyridine derivative, which is probably not brain-penetrant, in view of the structural similarity of ^{18}F-SynVesT-2 to ^{11}C-UCB-J and ^{18}F-SynVesT-1. The Food and Drug Administration–approved SV2A ligand levetiracetam blocked 85% of the specific binding of ^{18}F-SynVesT-2 in the human brain at an intravenous dose of 20 mg/kg. The extent of blockade is similar to that for ^{11}C-UCB-J and ^{18}F-SynVesT-1 (*5*). Interestingly, the estimated V_{ND}/f_p is 4.86 mL/cm^3, indicating that about 20% of the tracer uptake in CS at baseline is attributable to specific uptake, which is lower than the 35%–40% for ^{11}C-UCB-J (*2*). Note that the CS ROI we used has been optimized to minimize the spill-in effects from the surrounding gray matter (*2*). The source of the specific binding in CS remains elusive for the SV2A PET tracers. The volume changes in CS need to be accounted for in neurodegenerative diseases at advanced stages.

Because of the lower tracer uptake of ^{18}F-SynVesT-2 in CS, the lower 1TC V_T in gray matter did not lead to a dramatically lower BP_{ND}. We correlated the baseline V_T of ^{18}F-SynVesT-2 with that of ^{11}C-UCB-J and ^{18}F-SynVesT-1 in the same subjects. By assuming the same maximum available binding sites (B_{max}) for the 3 SV2A PET tracers in the same subjects, the in vivo K_d ratios of ^{18}F-SynVesT-2 to ^{11}C-UCB-J and ^{18}F-SynVesT-1 are 3 (Supplemental Fig. 6), which is similar to the in vitro K_d ratios measured using postmortem human brain tissue (*33*). Taken together, this indicates that the f_{ND} of ^{18}F-SynVesT-2 is higher than that of ^{11}C-UCB-J and ^{18}F-SynVesT-1. Though we did not experimentally measure the f_{ND} of these tracers, using the V_{ND} estimated from the baseline-blocking studies in 5 subjects and the corresponding f_p, we calculated the f_{ND} of ^{18}F-SynVesT-2 to be 0.17 ± 0.05 ($n = 6$), which is indeed higher than the calculated f_{ND} of ^{11}C-UCB-J (0.086) and ^{18}F-SynVesT-1 (0.13) (*5*).

TABLE 3
Test–Retest Reproducibility of Kinetic Parameters of ^{18}F-SynVesT-2 Derived with 1TC Model from 90 Minutes of Time–Activity Curves

	K_1 (mL/cm^3/min)				V_T (mL/cm^3)			
	TRV		aTRV		TRV		aTRV	
Region	Mean	SD	Mean	SD	Mean	SD	Mean	SD
Amygdala	0.50	9.69	6.63	6.27	−1.97	7.06	5.73	3.71
CS	2.88	8.62	7.71	3.22	−2.05	10.18	7.17	6.68
Caudate nucleus	−2.78	14.99	12.90	5.13	−4.29	6.83	6.14	4.75
Cerebellum	−3.72	12.91	10.28	7.20	−3.96	6.07	5.96	3.48
Frontal lobe	−1.32	12.14	8.81	7.26	−2.74	7.69	6.07	4.74
Hippocampus	−0.29	10.55	8.31	5.00	−0.31	6.69	5.35	3.03
Occipital lobe	1.20	12.82	8.76	8.37	−1.75	8.72	6.95	4.41
Parietal lobe	−1.47	11.93	9.59	5.50	−2.61	6.32	4.83	4.39
Putamen	−5.27	13.85	12.02	6.76	−3.11	7.03	6.39	3.23
Temporal lobe	−1.41	11.81	8.16	7.66	−1.90	8.16	6.12	4.93
Thalamus	−6.04	14.59	13.47	5.64	−2.56	5.31	4.69	2.97

Data are percentages. $n = 5$.

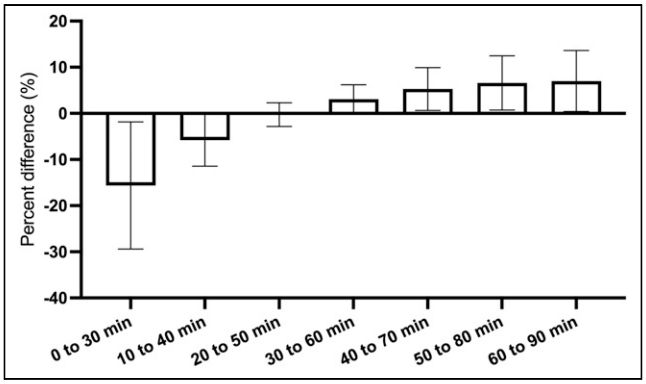

FIGURE 7. Percentage differences of SUVR–1 of ^{18}F-SynVesT-2 in different scan time windows from BP_{ND}, represented as mean and SD for each 30-min time window. Mean percentage difference for each imaging window is for 10 brain regions in 14 baseline scans. SD reflects variability of averaged percentage differences for different brain regions.

Shortening of the dynamic scan time from 2 h to 30 min had negligible impact (−0.3% ± 4.3%) on the BP_{ND} estimation for ^{18}F-SynVesT-2. This is significantly shorter than the 60 min required for ^{11}C-UCB-J and ^{18}F-SynVesT-1 (*5*). To simplify the scan protocol as static scanning that is easier to execute in multicenter clinical trials, we opted to use SUVR–1 as a surrogate for BP_{ND} by comparing the averaged SUVR–1 from different imaging windows with the BP_{ND} from the full 90-min dataset. We found that the optimal static imaging window is 20–50 min after injection, with −0.3% ± 2.6% difference between SUVR–1 from 20 to 50 min and BP_{ND}. Therefore, the fast pharmacokinetics of ^{18}F-SynVesT-2 requires only a 30-min dynamic scan to reliably derive K_1, V_T, and BP_{ND}, or a 30-min static scan (20–50 min after injection) to calculate the SUVR–1 as a surrogate of BP_{ND}. ^{18}F-FDG PET, as a surrogate measure of neuronal activity, has been extensively used in the early detection of Alzheimer disease (*34*). The kinetic parameter K_1 is proportional to the blood flow and extraction fraction and serves as an index of blood flow for tracers with high brain permeability and a constant extraction fraction throughout the brain (no leakage in the blood–brain barrier, and no active influx or efflux). Indeed, Chen et al. have previously demonstrated a strong correlation between the ^{11}C-UCB-J K_1 and ^{18}F-FDG K_i in 14 Alzheimer disease subjects and 11 cognitively normal controls (R^2 = 0.21–0.66) (*10*). Also, in another study on 7 healthy subjects, the K_1 of ^{11}C-UCB-J in the visual cortex was sensitive to changes in cerebral blood flow and correlated well with the functional MRI blood oxygenation level–dependent response, whereas the V_T and BP_{ND} were unchanged during visual stimulations (*35*). Use of a relatively short 30-min dynamic ^{18}F-SynVesT-2 PET scan to gather information on a patient's cerebral blood flow and synapse density, in lieu of a ^{18}F-FDG PET scan and an SV2A PET scan, is expected to have clinical practicality.

In the literature, SV2A PET has been associated with synaptic density measurement. However, as the function of SV2A remains elusive, the validity of using SV2A PET as a quantification method for synaptic density needs to be validated for each application scenario.

CONCLUSION

The newly developed SV2A PET tracer ^{18}F-SynVesT-2 has faster brain kinetics than ^{11}C-UCB-J and ^{18}F-SynVesT-1 and similarly excellent test–retest reliability. Although lower than that of ^{11}C-UCB-J and ^{18}F-SynVesT-1, the specific binding of ^{18}F-SynVesT-2 in the human brain remains high, as evidenced by a BP_{ND} in the range of 1.76 to 3.06. The fast kinetics and high specific binding of ^{18}F-SynVesT-2 in the brain allows shortened dynamic scans to get information related to both cerebral blood flow (K_1) and synapse density (V_T or BP_{ND}), which could potentially lead to improved imaging throughput and expanded patient populations.

DISCLOSURE

This research was supported by grants R01AG052560, R01AG065474, R01AG058773, and R01NS123183 from the National Institutes of Health and by research grants from the Michael J. Fox Foundation and the Archer Foundation. We thank the staff at the Yale PET Center for expert technical assistance. This publication was also made possible by CTSA grant UL1 RR024139 awarded jointly by the National Center for Research Resources (NCRR) and the National Center for Advancing Translational Sciences (NCATS), components of the National Institutes of Health (NIH). The contents of this publication are solely the responsibility of the authors and do not necessarily represent the official view of NIH. The radioligand ^{18}F-SynVesT-2 (formerly referred to as ^{18}F-SDM-2) is contained in the patent US11518754B2, "Radiolabeled Pharmaceuticals and Methods of Making and Using Same," filed on February 15, 2018, and granted on December 6, 2022 (Inventors: Yiyun Huang, Zhengxin Cai, Songye Li, Nabeel Nabulsi, and Richard Carson). No other potential conflict of interest relevant to this article was reported.

KEY POINTS

QUESTION: Do the fast kinetics and high specific binding of ^{18}F-SynVesT-2 in nonhuman primates translate to human brain PET?

PERTINENT FINDINGS: With high specific binding and fast and reversible kinetics in the human brain, ^{18}F-SynVesT-2 allows for shortened imaging protocols, higher imaging throughput, and expanded patient populations.

IMPLICATIONS FOR PATIENT CARE: With simplified and shortened scan protocols, ^{18}F-SynVesT-2 is expected to improve patient compliance while maximizing information obtained from a single dynamic PET scan.

REFERENCES

1. Takeuchi T, Duszkiewicz AJ, Morris RGM. The synaptic plasticity and memory hypothesis: encoding, storage and persistence. *Philos Trans R Soc Lond B Biol Sci.* 2013;369:20130288.
2. Rossano S, Toyonaga T, Finnema SJ, et al. Assessment of a white matter reference region for ^{11}C-UCB-J PET quantification. *J Cereb Blood Flow Metab.* 2020;40:1890–1901.
3. Finnema SJ, Nabulsi NB, Mercier J, et al. Kinetic evaluation and test-retest reproducibility of [^{11}C]UCB-J, a novel radioligand for positron emission tomography imaging of synaptic vesicle glycoprotein 2A in humans. *J Cereb Blood Flow Metab.* 2017;0:271678X17724947.
4. Li S, Naganawa M, Pracitto R, et al. Assessment of test-retest reproducibility of [^{18}F]SynVesT-1, a novel radiotracer for PET imaging of synaptic vesicle glycoprotein 2A. *Eur J Nucl Med Mol Imaging.* 2021;48:1327–1338.
5. Naganawa M, Li S, Nabulsi N, et al. First-in-human evaluation of ^{18}F-SynVesT-1, a radioligand for PET imaging of synaptic vesicle glycoprotein 2A. *J Nucl Med.* 2021;62:561–567.

6. Bahri MA, Plenevaux A, Aerts J, et al. Measuring brain synaptic vesicle protein 2A with positron emission tomography and [^{18}F]UCB-H. *Alzheimers Dement (N Y).* 2017;3:481–486.
7. Cai Z, Li S, Matuskey D, Nabulsi N, Huang Y. PET imaging of synaptic density: a new tool for investigation of neuropsychiatric diseases. *Neurosci Lett.* 2019;691:44–50.
8. Finnema SJ, Li S, Cai Z, et al. PET imaging of synaptic vesicle protein 2A. In: Dierckx RAJO, Otte A, de Vries EFJ, van Waarde A, Lammertsma AA, eds. *PET and SPECT of Neurobiological Systems.* Springer International Publishing; 2021:993–1019.
9. Spurrier J, Nicholson L, Fang XT, et al. Reversal of synapse loss in Alzheimer mouse models by targeting mGluR5 to prevent synaptic tagging by C1Q. *Sci Transl Med.* 2022;14:eabi8593.
10. Chen MK, Mecca AP, Naganawa M, et al. Comparison of [^{11}C]UCB-J and [^{18}F]FDG PET in Alzheimer's disease: a tracer kinetic modeling study. *J Cereb Blood Flow Metab.* 2021;0:271678X211004312.
11. Mecca AP, Chen M-K, O'Dell RS, et al. In vivo measurement of widespread synaptic loss in Alzheimer's disease with SV2A PET. *Alzheimers Dement.* 2020;16:974–982.
12. Chen MK, Mecca AP, Naganawa M, et al. Assessing synaptic density in Alzheimer disease with synaptic vesicle glycoprotein 2A positron emission tomographic imaging. *JAMA Neurol.* 2018;75:1215–1224.
13. Cai Z, Li S, Zhang W, et al. Synthesis and preclinical evaluation of an ^{18}F-labeled synaptic vesicle glycoprotein 2A PET imaging probe: [^{18}F]SynVesT-2. *ACS Chem Neurosci.* 2020;11:592–603.
14. Cristy M, Eckerman KF, Marietta M, Systems E. *Specific Absorbed Fractions of Energy at Various Ages from Internal Photon Sources.* Oak Ridge National Laboratory; 1987:1–110.
15. Stabin MG, Sparks RB, Crowe E. OLINDA/EXM: the second-generation personal computer software for internal dose assessment in nuclear medicine. *J Nucl Med.* 2005;46:1023–1027.
16. Carson RE, Barker WC, Liow J-S, Johnson CA. Design of a motion-compensation OSEM list-mode algorithm for resolution-recovery reconstruction for the HRRT. In: *2003 IEEE Nuclear Science Symposium. Conference Record*; IEEE; 2003:3281–3285.
17. Jin X, Mulnix T, Gallezot JD, Carson RE. Evaluation of motion correction methods in human brain PET imaging: a simulation study based on human motion data. *Med Phys.* 2013;40:102503.
18. Hilton J, Yokoi F, Dannals RF, Ravert HT, Szabo Z, Wong DF. Column-switching HPLC for the analysis of plasma in PET imaging studies. *Nucl Med Biol.* 2000;27:627–630.
19. Gallezot JD, Esterlis I, Bois F, et al. Evaluation of the sensitivity of the novel α4β2* nicotinic acetylcholine receptor PET radioligand 18F-(−)-NCFHEB to increases in synaptic acetylcholine levels in rhesus monkeys. *Synapse.* 2014;68:556–564.
20. Holmes CJ, Hoge R, Collins L, Woods R, Toga AW, Evans AC. Enhancement of MR images using registration for signal averaging. *J Comput Assist Tomogr.* 1998;22:324–333.
21. Tzourio-Mazoyer N, Landeau B, Papathanassiou D, et al. Automated anatomical labeling of activations in SPM using a macroscopic anatomical parcellation of the MNI MRI single-subject brain. *Neuroimage.* 2002;15:273–289.
22. Pajevic S, Daube-Witherspoon ME, Bacharach SL, Carson RE. Noise characteristics of 3-D and 2-D PET images. *IEEE Trans Med Imaging.* 1998;17:9–23.
23. Guo Q, Owen DR, Rabiner EA, Turkheimer FE, Gunn RN. A graphical method to compare the in vivo binding potential of PET radioligands in the absence of a reference region: application to [^{11}C]PBR28 and [^{18}F]PBR111 for TSPO imaging. *J Cereb Blood Flow Metab.* 2014;34:1162–1168.
24. Onwordi EC, Halff EF, Whitehurst T, et al. Synaptic density marker SV2A is reduced in schizophrenia patients and unaffected by antipsychotics in rats. *Nat Commun.* 2020;11:246.
25. Matuskey D, Tinaz S, Wilcox KC, et al. Synaptic changes in Parkinson disease assessed with in vivo imaging. *Ann Neurol.* 2020;87:329–338.
26. Finnema SJ, Toyonaga T, Detyniecki K, et al. Reduced synaptic vesicle protein 2A binding in temporal lobe epilepsy: a [^{11}C]UCB-J positron emission tomography study. *Epilepsia.* 2020;61:2183–2193.
27. Delva A, Van Weehaeghe D, Koole M, Van Laere K, Vandenberghe W. Loss of presynaptic terminal integrity in the substantia nigra in early Parkinson's disease. *Mov Disord.* 2020;35:1977–1986.
28. D'Souza DC, Radhakrishnan R, Naganawa M, et al. Preliminary in vivo evidence of lower hippocampal synaptic density in cannabis use disorder. *Mol Psychiatry.* 2021;26:3192–3200.
29. Holmes SE, Scheinost D, Finnema SJ, et al. Lower synaptic density is associated with depression severity and network alterations. *Nat Commun.* 2019;10:1529.
30. Finnema SJ, Nabulsi NB, Eid T, et al. Imaging synaptic density in the living human brain. *Sci Transl Med.* 2016;8:348ra96.
31. Wilson H, Pagano G, de Natale ER, et al. Mitochondrial complex 1, sigma 1, and synaptic vesicle 2A in early drug-naive Parkinson's disease. *Mov Disord.* 2020;35:1416–1427.
32. O'Dell RS, Mecca AP, Chen M-K, et al. Association of Aβ deposition and regional synaptic density in early Alzheimer's disease: a PET imaging study with [^{11}C]UCB-J. *Alzheimers Res Ther.* 2021;13:11.
33. Patel S, Knight A, Krause S, et al. Preclinical in vitro and in vivo characterization of synaptic vesicle 2A-targeting compounds amenable to F-18 labeling as potential PET radioligands for imaging of synapse integrity. *Mol Imaging Biol.* 2020;22:832–841.
34. Mosconi L. Glucose metabolism in normal aging and Alzheimer's disease: methodological and physiological considerations for PET studies. *Clin Transl Imaging.* 2013;1:10.1007/s40336-013-0026-y.
35. Smart K, Liu H, Matuskey D, et al. Binding of the synaptic vesicle radiotracer [^{11}C]UCB-J is unchanged during functional brain activation using a visual stimulation task. *J Cereb Blood Flow Metab.* 2021;41:1067–1079.